Surface Chemistry Of Disordered Mackinawite (FeS)

Mariëtte Wolthers[1][*], Laurent Charlet[2], Peter R. van der Linde[3], David Rickard[4], and

Cornelis H. van der Weijden[1]

[1]Department of Earth Sciences – Geochemistry, Faculty of Geosciences, Utrecht University,

Utrecht, The Netherlands.

[2]L.G.I.T., Université Grenoble I, Grenoble, France.

[3]University of Professional Education Leiden, The Netherlands.

[4]School of Earth, Ocean and Planetary Sciences, Cardiff University, Cardiff, Wales, U.K.

[*] E-mail: wolthers@geo.uu.nl

ABSTRACT

Disordered mackinawite, FeS, is the first formed iron sulfide in ambient sulfidic environments and has a highly reactive surface. In this study, the solubility and surface chemistry of FeS is described. Its solubility in the neutral pH-range can be described by $K_S^{app} = \{Fe^{2+}\} \cdot \{H_2S(aq)\} \cdot \{H^+\}^{-2} = 10^{+4.87 \pm 0.27}$. Acid–base titrations show that the point of zero charge (PZC) of disordered mackinawite lies at pH ~7.5. The hydrated disordered mackinawite surface can be best described by strongly acidic mono-coordinated and weakly acidic tri-coordinated sulfurs. The mono-coordinated sulfur site determines the acid–base properties at pH < PZC and has a concentration of 1.2×10^{-3} mol per gram FeS. At higher pH, the tri-coordinated sulfur, which has a concentration of 1.2×10^{-3} mol per gram FeS, determines surface charge changes. Total site density is 4 sites nm^{-2}. The acid–base titration data are used to develop a surface complexation model for the surface chemistry of FeS.

1. INTRODUCTION

Disordered mackinawite is a highly reactive phase with a high adsorptive capacity for divalent metals (e.g., Kornicker, 1988; Arakaki and Morse, 1993; Morse and Arakaki, 1993; Wharton et al., 2000). Anoxic marine sediment pore waters are saturated with respect to disordered mackinawite (Berner, 1967; Spadini et al., 2003). It is the first iron sulfide to form in most ambient environments and with time it reacts to form more stable iron sulfide phases such as ordered mackinawite, greigite and ultimately pyrite or pyrrhotite. In this paper, disordered mackinawite is defined as the first precipitated iron(II) monosulfide phase formed through the reaction between aqueous Fe(II) and sulfide under ambient conditions. Lennie and Vaughan (1996) showed that this phase, which is sometimes referred to as "amorphous FeS", displays long-range mackinawite ordering. Here, this phase is referred to as FeS.

The bulk structure of FeS was studied by Wolthers et al. (2003) by X-ray powder diffraction measurements. They showed that synthetic FeS displays a disordered tetragonal mackinawite structure and that it is nanocrystalline, with an average primary particle size equivalent to a crystallite size of 4 nm and a corresponding specific surface area of 350 $m^2 g^{-1}$ (Table 1). FeS was described in terms of a mixture of two end-member phases with different long-range ordering, with the relative proportions of the end-members varying with age and, probably, with formation conditions. Lattice expansions of up to 54 vol.% relative to crystalline mackinawite were explained by intercalation of water molecules between the tetrahedral sheets and by lattice relaxation due to small crystallite size.

Fundamental surface chemical properties have not been reported for disordered mackinawite. In fact, experimental characterization studies of sulfide surfaces are rare in general, despite the accepted importance of the reactivity of sulfides in the geochemical cycles of many trace

elements (e.g., Kornicker, 1988; Arakaki and Morse, 1993; Morse and Arakaki, 1993; Morse and Luther, 1999; Wharton et al., 2000). With the notable exception of the structural and magnetic study by Watson et al. (2000) on an iron sulphide mixture of disordered mackinawite and greigite, that was formed by sulfate-reducing bacteria, all recent studies aiming to describe the surface properties of metal sulfides, pertained to the more crystalline solid. Potentiometrically derived point of zero charge (pH_{PZC}) data are available for crystalline iron sulfides (Widler and Seward, 2002), zinc sulfide (Rönngren et al., 1991), lead sulfide (Sun et al., 1991), arsenic and antimony sulfide (Renders and Seward, 1989), and for cadmium sulfide (Park and Huang, 1987). Dekkers and Schoonen (1994) and Bebié et al. (1998) employed electrophoresis to study the charge development of sulfides as a function of pH. They found that the isoelectrical points for several crystalline metal sulfides lie below pH ~3.3 and showed that the sulfide surface was largely dominated by sulfide groups.

The objective of this study is to describe the experimentally determined surface properties of synthetic FeS produced by reacting aqueous Fe(II) with aqueous sulfide. The solubility of FeS in the neutral pH range is addressed and the acid–base properties of the FeS surface are characterized using potentiometric titrations. Subsequently, the potentiometric titration data are used to propose a surface complexation model, which is supported by crystal structural considerations.

2. MATERIALS AND METHODS

2.1. Materials

All chemicals were of analytical grade and used without further purification; solutions were prepared from Milli-Q^{TM} water and purged for at least 30 minutes with O_2-free N_2 before use. Solutions of S(–II) and Fe(II) were prepared before every experiment by dissolving $Na_2S \cdot 9H_2O$ (Fisher Chemicals^{TM}) and Mohr's salt ($Fe(NH_4)_2(SO_4)_2 \cdot 4H_2O$; Merck^{TM}), which is relatively resistant to oxidation, in background electrolyte of varying KNO_3 (Fisher Chemicals^{TM}) concentration. Because the salt are hydrates, the Fe and S concentrations were checked regularly by ICP–OES analysis, where the Na concentration in the sulfide solution was assumed representative of the sulfide concentration.

Experiments were run under O_2-free conditions by directly flushing the reaction vessel with N_2, purified by bubbling through a succession of two 15 wt.% pyrogallol in 50 wt.% KOH solutions to remove O_2, a Chrompack^{TM} oxygen and sulfide scrubber for additional cleaning and Milli-Q^{TM} water to saturate the N_2 with water vapor. The O_2 concentration in the reaction vessels was below 1×10^{-6} M, which is the detection limit of the Orion^{TM} oxygen probe (850).

Fresh FeS suspensions for potentiometric titrations was synthesized in situ by adding a 1×10^{-3} M S(–II) solution to a 1×10^{-3} M Fe(II) solution in the reaction vessel while constantly flushing with N_2. FeS formed rapidly and was left to age in the reaction vessel for at least half

an hour before the initial pH was set, and one hour before experimentation started. The suspensions were stirred magnetically with a Teflon^{TM}-coated stirring bar.


2.2. Solubility

Since the solubility will depend on the method of synthesis (e.g. Davison, 1991) and dissolution of the solid will influence the proton balance determined in the potentiometric titration, the solubility of the synthetic FeS used in this study needs to be determined. Note that all species are aqueous unless otherwise indicated and that equilibrium is assumed between all solution species and with the solid.

The solubility of FeS can be expressed by reaction (1):

(1)
$$FeS(s) + 2H^+ \leftrightarrow Fe^{2+} + H_2S(aq) \qquad K_S^{app}$$
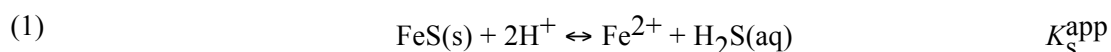
K_S^{app} is the apparent solubility constant at zero ionic strength which is derived from the experimental pH and total dissolved Fe data and compared to the solubility $K_S^* = 10^{+3.98\pm0.12}$ from Davison et al. (1999), recalculated from their $K_S^* = \{Fe^{2+}\}\cdot\{HS^-\}\cdot\{H^+\}^{-1}$ $= 10^{-3.00\pm0.12}$ by using $K_1 = \{H_2S(aq)\}\cdot\{HS^-(aq)\}^{-1}\cdot\{H^+(aq)\}^{-1} = 10^{+6.98}$ (Suleimonov and Seward, 1997). A 1:1 iron to sulfide stoichiometry is assumed based on EDX spectra collected on freeze-dried FeS particles (Wolthers et al., 2003). Furthermore, dissolution is assumed to be congruent. The aqueous sulfide chemistry is represented by the following reactions:

(2)
$$H_2S(aq) \leftrightarrow HS^- + H^+ \qquad K_1$$
(3)
$$H_2S(g) \leftrightarrow H_2S(aq) \qquad K_H$$
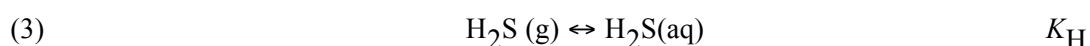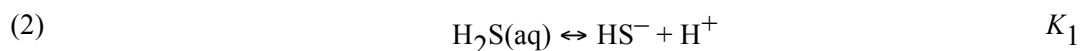
where $K_1 = 10^{-6.98}$ (Suleimonov and Seward, 1997) and $K_H = \{H_2S(aq)\}P_{H2S}^{-1} = 10^{+0.99}$ (Morel and Hering, 1993) at zero ionic strength. A closed-system equilibrium with respect to hydrogen sulfide gas is assumed. Calculation shows that, at a conservatively estimated

purging rate of 100 mL per minute, within the time frame of our experiments (< 42 hr) 0.1 %

of the sulfide present would degas if the system would have been at pH 6 continuously and at

pH 8, this decreases to 0.0003 %. In reality, the titration cell was only briefly at pH 6 (<1

hour) and the average time of titration experiments was 8 hours, 40 minutes.. Accordingly,

reaction (3) will be ignored in further calculations.

Aqueous iron–sulfide complexation plays an important role in this pH range (Rickard, 1989;

Davison, 1991; Luther, 1991; Luther and Ferdelman, 1993; Zhang and Millero, 1994;

Rickard, 1995; Luther et al., 1996; Davison et al, 1999). The two most simple complexation

reactions reported are:

(4) $$FeS(s) + H^+ \leftrightarrow FeSH^+ \qquad \beta_1$$

(5) $$FeS(s) + H_2S(aq) \leftrightarrow Fe(SH)_2^0 \qquad \beta_2$$
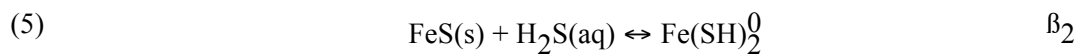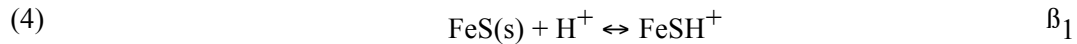
where $\beta_1 = 10^{+2.05\pm0.5}$ (Luther et al., 1996), $\beta_2 = 10^{-3.43\pm0.1}$ (Davison et al., 1999). The

way reactions (4), (5) and (1) are written simplifies further derivations; no assumptions about

the actual reactive species or reaction mechanisms are made. Davison et al. (1999) determined

a much lower value for β_1, i.e. $\beta_1 = 10^{+0.05\pm0.1}$. There is still considerable disagreement on

aqueous iron–sulfide complexation reactions and their thermodynamic constants, the latter

should therefore be treated with caution (Davison et al., 1999). It may be that the iron–sulfide

complexation is sensitive to FeS characteristics, which in turn are sensitive to the preparation

method (Davison, 1991). Since in this study FeS was prepared using the same method as

Luther et al. (1996), their higher β_1 value is adopted.

From (1) to (5) the definitions for the activities of the sulfide species and aqueous iron(II)–

sulfide complexes can be derived:

(6) $${H_2S(aq)} = \frac{K_s^{app} \{H^+\}^2}{\{Fe^{2+}\}}$$

(7)
$$\{HS^-\} = \frac{K_1 \{H_2S(aq)\}}{\{H^+\}} = \frac{K_1 \, K_S^{app} \, \{H^+\}}{\{Fe^{2+}\}}$$

(8)
$$\{FeSH^+\} = \beta_1 \{H^+\}$$

(9)
$$\{Fe(SH)_2^0\} = \beta_2 \{H_2S(aq)\} = \frac{\beta_2 \, K_S^{app} \, \{H^+\}^2}{\{Fe^{2+}\}}$$

Furthermore, the expressions for total iron (10) and total sulfide (11) in the system are known and it is assumed that the two are equal as a first approximation (12):

(10)
$$Fe_T = [Fe^{2+}] + [FeSH^+] + [Fe(SH)_2^0] + [FeS(s)]$$

(11)
$$S_T = [HS^-] + [H_2S(aq)] + [FeSH^+] + 2[Fe(SH)_2^0] + [FeS(s)]$$

(12)
$$[Fe^{2+}] = [HS^-] + [H_2S(aq)] + [Fe(SH)_2^0]$$

Combining (6) to (12), an expression for the Fe(II) activity is obtained as follows:

(12b)
$$\frac{\{Fe^{2+}\}}{\gamma_{Fe}} = \frac{\{H_2S(aq)\}}{\gamma_{H2S}} + \frac{\{HS^-\}}{\gamma_{HS}} + \frac{\{Fe(SH)_2^0\}}{\gamma_{Fe(SH)_2}}$$

(12c)
$$\frac{\{Fe^{2+}\}}{\gamma_{Fe}} = \frac{K_S^{app} \, \{H^+\}^2}{\gamma_{H2S}\{Fe^{2+}\}} + \frac{K_1 \, K_S^{app} \, \{H^+\}}{\gamma_{HS}\{Fe^{2+}\}} + \frac{\beta_2 \, K_S^{app} \, \{H^+\}^2}{\gamma_{Fe(SH)_2}\{Fe^{2+}\}}$$

(13)
$$\{Fe^{2+}\} = \sqrt{\gamma_{Fe} \, K_S^{app} \left(\frac{\{H^+\}^2}{\gamma_{H2S}} + \frac{K_1\{H^+\}}{\gamma_{HS}} + \frac{\beta_2\{H^+\}^2}{\gamma_{Fe(SH)_2}} \right)}$$

To compare the experimental solubility to the literature solubility, it is assumed that the total dissolved iron, $[Fe(aq)_T]$, can be equated by:

(14)
$$[Fe(aq)_T] = [Fe^{2+}] + [FeSH^+] + [Fe(SH)_2^0]$$

Substituting equations (8), (9) and (13) into (14) and taking the literature values for the equilibrium constants, equation (14) can be solved for any pH value. Extrapolation to zero theoretical ionic strength (cf. Davison, 1991) facilitates comparison of the solubility calculated here to the literature solubility; the corrections of the experimental titration data is done with the appropriate activity coefficients. The K_S^{app} was determined by the best fit

method, calculated by multiple least-squares estimation and multiple linear correlation; the error in the solubility constant was taken as twice the standard error of estimate.

2.3. Surface Characterizations

The aim of the potentiometric titration was to determine the balance of adsorbed and desorbed protons on the surface of the disordered mackinawite as a function of pH, within the pH range of 6 to 8. The FeS titrations were conducted on in situ precipitated FeS, thus in a background electrolyte solution containing sodium, sulfate and ammonium as well as the 0.005 M, 0.05 M, or 0.1 M KNO_3 ionic medium, giving total ionic strengths of 0.0078 M, 0.053 M, or 0.103 M. The titrations were performed from pH 8 to 6 to prevent back precipitation reactions to occur as pH increases (the FeS solubility decreases with increasing pH). This would have interfered with the surface acid–base reactions. Afterwards, reversibility of the titrations was tested by increasing the pH back to 8. The freshly precipitated 0.044 g L^{-1} FeS suspension was prepared as described above and kept at 23.2 ± 0.4°C. In the course of the titrations, 1 mL samples were taken from the suspension and filtered through 0.2 μm Acrodisc[TM] filter discs. The total dissolved iron in the filtrates was measured spectrophotometrically by the ferrozine method (Viollier et al., 2000) using a Unicam[TM] UV1 spectrophotometer, to check for mineral dissolution during titrations. FeS was shown to be nano-meter sized (Wolthers et al., 2003), and it is likely that the efficiency of the filtration process was affected by the small particle size.

Two blank titrations were performed on supernatants which had been collected after filtrating FeS suspensions at pH 8 or 6 through a 0.2 μm Millipore[TM] filter. In this way, not only contributions to the surface charge by matrix species is accounted for, but also possible contributions by equilibrium concentrations of Fe(II) and sulfide, which increase with decreasing pH, are taken into account. The pH 8 supernatant was titrated to pH 6 and back to

8; the pH 6 supernatant was titrated to pH 8. No significant difference between the two blanks was found, so for blank corrections the data from the blank titration performed down to pH 6 after filtration of the suspension at pH 8 were used.

The pH of the suspension in the air-tight 500 mL titration cell was controlled via an automated system, consisting of a Metrohm^{TM} 736 GP Titrino for base delivery ([NaOH] = 0.01 M) and a Metrohm^{TM} 685 Dosimat for acid delivery ([HCl] = 0.1 M) coupled to a PC equipped with TiNet$^{©}$ 2.4 software. In order to minimize local OH^- or H^+ excess, acid and base were added at a rate of 0.05 mL min^{-1}. Throughout the experiment, pH was measured using a Metrohm^{TM} 6.0233.100 combined LL pH glass electrode incorporated in the titration cell. Prior to use, the electrode was calibrated in CALITECH^{TM} pH 4, 7 and 10 buffers traceable to NIST (National Institute of Standards and Technology) standards and after use, the electrode was checked for drift in the pH 7 buffer. The drift of the electrode during a run was always less than 0.01 pH unit. The pH of the suspension had been adjusted to an initial value of 8 by base addition, before the potentiometric titration was started. Titrations were performed by decreasing the pH to a value of 6 and then back to a value of 8. After each acid or base addition, the pH reading was allowed to stabilize before the next addition. A potential drift of less then 0.5 mV min^{-1} was used as a criterion for stable readings, or a maximum equilibration time of 30 minutes was allowed if a stable reading was not reached.

The proton balance on the solid surface, Q (in mol per g FeS), was calculated from the potentiometric acid titration by correcting the total proton balance in the system ($C_A - C_B$) for all matrix impurities and dissolution of the solid as follows:

(15)
$$Q = \frac{C_A - C_B - Q_{blank} - [H^+]_c}{N}$$

10

where C_A and C_B are acid and base concentrations added per liter, N is the amount of solid (in g L^{-1}). Q_{blank}, in M, is the proton balance as a function of pH derived from the blank potentiometric titration as follows (Stumm, 1991):

(16)
$$Q_{\text{blank}} = C_A - C_B + [\text{OH}^-] - [\text{H}^+]$$

Q_{blank} includes all protolytic components in the matrix such as ammonia and aqueous bisulfide. The H$^+$ concentration is calculated from the measured pH and $[\text{OH}^-] = K_w \{\text{H}^+\}^{-1} \gamma_{\text{OH}}^{-1}$. The term $[\text{H}^+]_c$ in equation (15) describes the proton consumption by solid dissolution depending on pH. This correction of Q is necessary because of the high solubility of FeS, especially towards lower pH values (cf. Schulthess and Sparks, 1986; Bayens and Bradbury, 1997). In order to derive an expression for $[\text{H}^+]_c$, a mass balance relating the consumed protons to the produced Fe(II) and S(–II) species needs to be made (17):

(17)
$$[\text{H}^+]_c = [\text{HS}^-]_p + 2[\text{H}_2\text{S(aq)}]_p + [\text{FeSH}^+]_p + 2[\text{Fe(SH)}_2^0]_p$$

For each bisulfide and FeSH$^+$ complex produced during dissolution one proton is consumed; for each H$_2$S(aq) and Fe(SH)$_2^0$ produced two protons are consumed. Combining mass balances (12) and (17) results in (18):

(18)
$$[\text{H}^+]_c = [\text{Fe}^{2+}] - [\text{Fe}^{2+}]_i + [\text{H}_2\text{S(aq)}] - [\text{H}_2\text{S(aq)}]_i + [\text{FeSH}^+] - [\text{FeSH}^+]_i + [\text{Fe(SH)}_2^0]$$

$$- [\text{Fe(SH)}_2^0]_i$$

where suffix c indicates consumed, p indicates produced by dissolution and i indicates initially in solution, i.e. at pH 8. Converting mass balance (18) to include activities for all species and filling in (6), (8), (9) and (13), an expression for $[\text{H}^+]_c$ can be derived as follows:

(18b)
$$\frac{\{\text{H}^+\}_c}{\gamma_\text{H}} = \frac{\{\text{Fe}^{2+}\}}{\gamma_\text{Fe}} - \frac{\{\text{Fe}^{2+}\}_i}{\gamma_\text{Fe}} + \frac{\{\text{H}_2\text{S(aq)}\}}{\gamma_\text{H2S}} - \frac{\{\text{H}_2\text{S(aq)}\}_i}{\gamma_\text{H2S}} + \frac{\{\text{FeSH}^+\}}{\gamma_\text{FeSH}} - \frac{\{\text{FeSH}^+\}_i}{\gamma_\text{FeSH}} +$$

$$\frac{\{\text{Fe(SH)}_2^0\}}{\gamma_{\text{Fe(SH)}2}} - \frac{\{\text{Fe(SH)}_2^0\}_i}{\gamma_{\text{Fe(SH)}2}}$$

(19)

$$[H^+]_c = \sqrt{\frac{K_S^{app}}{\gamma_{Fe}} \left(\frac{\{H^+\}^2}{\gamma_{H2S}} + \frac{K_1\{H^+\}}{\gamma_{HS}} + \frac{\beta_2\{H^+\}^2}{\gamma_{Fe(SH)_2}} \right)} - \frac{\{Fe^{2+}\}_i}{\gamma_{Fe}} +$$

$$\frac{K_S^{app}\{H^+\}^2}{\sqrt{\gamma_{Fe}\, K_S^{app} \left(\frac{\{H^+\}^2}{\gamma_{H2S}} + \frac{K_1\{H^+\}}{\gamma_{HS}} + \frac{\beta_2\{H^+\}^2}{\gamma_{Fe(SH)_2}} \right)}} - \frac{\{H_2S(aq)\}_i}{\gamma_{H2S}} + \frac{\beta_1\{H^+\}}{\gamma_{FeSH}} - \frac{\{FeSH^+\}_i}{\gamma^{FeSH}} +$$

$$\frac{\beta_2\, K_S^{app}\{H^+\}^2}{\gamma_{Fe(SH)_2}\sqrt{\gamma_{Fe}\, K_S^{app} \left(\frac{\{H^+\}^2}{\gamma_{H2S}} + \frac{K_1\{H^+\}}{\gamma_{HS}} + \frac{\beta_2\{H^+\}^2}{\gamma_{Fe(SH)_2}} \right)}} - \frac{\{Fe(SH)_2^0\}_i}{\gamma_{Fe(SH)_2}}$$

where $\{Fe^{2+}\}_i = 10^{-5.45}$, $\{H_2S(aq)\}_i = 10^{-6.51}$, $\{FeSH^+\}_i = 10^{-5.95}$ and $\{Fe(SH)_2^0\}_i =$

$10^{-9.9}$. With this expression (19), the amount of protons consumed can be calculated at any

pH for all ionic strengths by dissolution of synthetic FeS. All activity corrections were

calculated using the Davies equation. In the pH range of the experiments, the increase in

solution species due to dissolution of the solid has a negligible effect on the ionic strength.

Thus, the activity coefficients remain constant up to two decimals over the pH ranges of all

experiments.

3. RESULTS

3.1. Solubility

Fig. 1 shows the total dissolved Fe(II), $\log[\text{Fe(aq)}_T]$, with pH. The total dissolved iron, including both free and complexed Fe(II), was measured in aliquots taken during the titrations. The total dissolved iron increased with decreasing pH due to dissolution of the solid. Equation (14) is the expression for the total dissolved iron as a function of pH. The dotted line in Fig. 1 describes the calculated total dissolved iron as a function of pH if it is assumed that (i) equilibrium is established between all solution species and with the solid, (ii) H_2S degassing is insignificant, (iii) FeS is stoichiometric (cf., Lennie and Vaughan, 1996) and (iv) FeS dissolves congruently according to reaction (1) with an apparent solubility constant of $K_S^{\text{app}} = 10^{+3.98 \pm 0.12}$ (Davison et al., 1999). To fit the measured total dissolved iron concentrations, the value for K_S^{app} was varied by trial and error. The best fit was found with $K_S^{\text{app}} = 10^{+4.87 \pm 0.27}$, fitting the total dissolved iron data with an R^2 of 0.90, resulting in the band of solid lines in Fig. 1. This is higher than the value recalculated from Davison et al. (1999).

13

3.2. Potentiometric Titrations

The proton balances from the acid–base titrations were calculated through equation (15), that is, they have been corrected for proton consumption by: (i) protolytic components in solution, (ii) the dissociation of water, (iii) solid dissolution using $K_S^{app} = 10^{+4.87}$ and (iv) aqueous iron–sulfide complexation. Therefore, the surface protonation data, plotted as Q in mmol per gram FeS versus pH as circle, triangle and square symbols in Fig. 2a and 2b, represent the proton balances at the surface of disordered mackinawite at 0.053, 0.0078, or 0.103 M ionic strength. Since these surface protonation curves have a common inflection point at pH value: 7.5 ± 0.2, they have been shifted vertically so as to intersect each other and the Q = 0 mmol g^{-1} FeS at the common inflection point. This common inflection point is assumed to be the pH value where the surface has a zero proton charge (pH_{PZC}). Thus, at pH > ~7.5 the surface becomes increasingly negatively charged, approaching saturation at high pH values. At pH < ~7.5 the surface becomes increasingly positively charged until the surface approaches saturation at pH ≈ 6.5 (Fig. 2a and 2b). Significant hysteresis was observed between consecutive acid and base titrations (data not shown); the base titration was shifted as much as 1.5 pH unit higher than the acid titration.

4. DISCUSSION

4.1. Solubility

The solubility of FeS was determined in order to correct for dissolution effects during the acid–base titrations. The derived apparent solubility constant is K_S^{app} = {Fe^{2+}}·{$H_2S(aq)$}·{H^+}$^{-2}$ = $10^{+4.87\pm0.27}$ (25°C). Benning et al. (2000) noted that the solubility of FeS in the important neutral and alkaline pH range (6 > pH < 8.5) was poorly constrained and found values for K_S^{app} at 80°C of $10^{+6.55}$ (pH 8.15) and $10^{+7.31}$ (pH 7.39). The divergence observed at 25°C and pH 6–8 for K_S^{app} in the present study is, therefore, well within the uncertainty observed at 80°C at pH 7–8. Benning et al. (2000) also noted that the variation in their measurements in this pH range suggested that a detailed study of FeS solubility at neutral to alkaline pH was urgently required. Although not a detailed study, the present solubility determination for FeS is the first to result in a designation of K_S^{app} at neutral to alkaline pH.

The apparent solubility constant derived here is higher than the 20°C solubility constant K_S^* = $10^{+3.98\pm0.12}$ recalculated from Davison et al. (1999) (Fig. 1). Preparation methods have often been named as controlling bulk characteristics as, for example, particle size (cf. Morse et al, 1987; Davison, 1991; Wolthers et al., 2003) and, consequently, may control FeS reactivity and solubility. Furthermore, Wolthers et al. (2003) have shown that FeS may contain variable amounts of structurally incorporated water molecules, a property which is likely to influence solubility.

The total dissolved iron versus pH plot presented here (Fig. 1) shows a pH dependence of log[Fe(aq)$_T$] with an approximate average slope of –0.5 when fitted linearly. When reactions (1) controls FeS solubility in the pH 6–8 range, then the slope in Fig. 1 would be –1, assuming that {Fe^{2+}(aq)} is equal to {H$_2$S(aq)}. Similarly, when reactions (1) and (2) control FeS solubility, then the slope is –0.5. Furthermore, if the complexation reactions (4) or (5) would control FeS solubility, then the slope would be –1 or –2, respectively. However, while the average slope observed is –0.5, a close inspection of Fig. 1 shows that the slope tends to level off towards zero with increasing pH. In fact, this leveling off with pH suggests that the aqueous FeS cluster complex forms an important part of the total dissolved iron with increasing pH, because its formation is pH independent (Rickard and Luther, 1997):

(20)   FeS(s)$\rightarrow$ FeS(aq)

Furthermore, the size of the aqueous FeS cluster complex is too small to allow removal by filtration through the 0.2 µm filter discs used (cf. Wolthers et al., 2003). Therefore, from Fig. 1, it is concluded that the solubility is not simply controlled by one of the reactions (1), (2), (4) or (5), and that the dominant dissolution reaction changes with pH. Determining the dissolution mechanism or the generic solubility product for FeS in the neutral to alkaline pH range, is beyond the scope of the present work. The determined K_S^{app} allows correction for proton consumption during the potentiometric titration and, thus, serves the present purpose.

4.2. Surface Charge

Titrations performed with suspensions of in situ precipitated stoichiometric iron(II) monosulfide have the advantage of minimizing surface oxidation. The conditions can be kept as oxygen free as possible and any treatment such as drying which may alter the surface characteristics is avoided (Herbert et al., 1998; Morse and Arakaki, 1993). The precipitation process results in very small particles, implying a large surface area, which will simulate closely naturally occurring disordered mackinawite. It is expected that titrations performed in

solutions with increasing ionic strengths give an increasing slope of the resulting Q versus pH curve (c.f. Dzombak and Morel, 1990). However, the Q versus pH curves in Fig. 2a and 2b do not show this trend. The precipitation of FeS occurs through heterogeneous nucleation, forming a mixture of two end-member phases with different long-range crystallographic ordering and different sizes, followed by growth including lattice contractions and a change in relative proportions of the end-member phases (Wolthers et al., 2003). The variability of the titration data may be reflecting this complex stochastic precipitation process.

The trend from the surface protonation curves is nevertheless reproducible, showing an increase in surface charge with decreasing pH and reaching saturation towards high and low pH (Fig. 2a and 2b). When only one symmetrical inflection is observed in a solid titration curve, as with hydrous ferric oxide titrations, then the net surface protonation curve represents the protonation of one kind of active surface site. The pH value of this inflection point is assumed to be the pH_{PZC}. Moreover, in the numerous FeS syntheses performed during this study, the supernatant pH was observed to be stable within several minutes after precipitation at a value varying between 7.4 and 7.8. For carbonates, it has been shown that, when solubility equilibrium is attained, the electro neutrality condition applies to pH and the solutes in equilibrium with the solid carbonates ("proton condition", c.f. Stumm and Morgan, 1981; Van Cappellen et al., 1993). Stumm and Morgan postulated that under these conditions, the mineral suspension must have zero surface charge. Extrapolating the "proton condition" to iron sulfides, the observations of a stable supernatant pH support a pH_{PZC} ~7.5. If the surface charge is solely acquired by protonation and deprotonation, the point of zero charge is pristine and therefore equal to the pH_{PZNPC} (Dzombak and Morel, 1990). The FeS surface titrations were performed within a complex solution and adsorption of other potential determining ions cannot be ruled out. Therefore, the common inflection point of the surface protonation curves is referred to as the pH_{PZC}.

17

Significant hysteresis was observed between consecutive acid and base titrations; the base titration was shifted as much as 1.5 pH unit higher than the acid titration. For hydrous ferric oxide, similar hysteresis is observed. Sorption and desorption on oxides are governed by two-step kinetics: a fast initial step (minutes) followed by a much slower second step (Dzombak and Morel, 1990). The second step is generally thought to result from exchange within the interior of oxide particles, causing hysteresis between consecutive acid and base titrations. Rapid titrations should therefore be employed, that is, slow enough for the first step to reach equilibrium while fast enough to avoid the second step (c.f. Charlet et al., 1990). Even with fast acid–base titrations, hysteresis is observed. In particular, hysteresis is reported for amorphous oxides where the second step is faster than for more crystalline oxides (Dzombak and Morel, 1990). The fact that similar hysteresis is observed for FeS suggests that similar two-step kinetics govern the surface protonation and deprotonation reactions.

Widler and Seward (2002) performed the only previously reported potentiometric titration on the surface of mackinawite. They obtained a similarly shaped trend with one inflection, shifted to lower pH compared to Fig. 2a–b for hydrothermally synthesized and hence more crystalline mackinawite. They estimated the pH_{PZC} to be 2.9 for from one blank-uncorrected curve. However, no surface deprotonation was found in the base titration, that is, the surface protonation was irreversible, and they observed a surface protonation in zero ionic strength solutions only. These observations seem to be inconsistent with the data presented here and data for other mineral surfaces. In an electrokinetic study performed on a range of crystalline metal sulfides, although not on mackinawite, Bebié et al. (1998) estimated that the isoelectrical point ($pH_{i.e.p.}$, the point of zero charge in the shearing plane of the moving particle (Sposito, 1984)), for all studied metal sulfides lies below pH 3.3. In general, more alkaline points of zero charge, such as e.g. ~8.5 for ZnS from Rönngren et al. (1991), ~8.5 for PbS from Sun et al. (1991), ~7.7 for CdS from Park and Huang (1987) are thought to be affected by oxidation (Bebié et al., 1998; Widler and Seward, 2002), and the effect of slight

18

oxidation has been shown to shift the pH_{PZC} of pyrite (Bebié et al., 1998). Although it could be argued that the data reported here have been affected by oxidation as well, it should be noted that continuous dissolution of FeS during the titration renews the FeS surface while also increasing the S(–II) concentration in solution. The dissolved S(–II) may be more reactive towards O_2 than the FeS surface and further ensure anoxia. Therefore, it is assumed that the reproducible trends observed and the pH_{PZC} estimated are accurate and unaffected by oxidation. Moreover, discrepancies between proton titration data and electrokinetic data have been reported for other minerals, e.g. silica (Gabriel et al., 2001). The zeta potential, calculated from electrophoretic measurements, reflects the charge of the moving particle at the shearing plane, located in the diffuse layer at a distance from the surface (Sposito, 1984; Stumm, 1991). In contrast, from potentiometric titration data, the charge at the surface is calculated. Additionally, the FeS was precipitated in situ, and other components of the reactants, most notably sulfate, were not removed. The sorption of such components on the surface will affect the protonation/deprotonation and resulting surface charge and can shift the resulting pH_{PZC}. For example, Bebié et al. (1998) showed significant changes in, and indeed charge reversals of, the surface-charge pH-dependence with the addition of Fe(II) to a pyrite suspension. Hence, a difference between the values for the $pH_{i.e.p.}$ referred to above and the pH_{PZC} reported here for the same, though less crystalline, mineral surface is to be expected.

Features that might affect the pH_{PZC} of disordered mackinawite more strongly than of crystalline mackinawite are proton diffusion and ageing. Proton diffusion from the surface into the solid, e.g. in between the tetrahedral sheets, as indicated by the hysteresis of the acid and base titrations, leads to an overestimated surface charge since the surface explored by protons increases with time (Dzombak and Morel, 1990). Thus, the pH_{PZC} will be shifted to a more alkaline pH due to proton diffusion. This may be expected to be important for FeS, since FeS has been shown to contain intercalation of water, or possibly OH^-, molecules the

19

tetrahedral sheets (Wolthers et al., 2003). Significantly lower pH_{PZC} values were reported for hydrous ferric oxide after long ageing times (Prasad, 1976; Kuo and McNeal, 1984) with the possibility of transformation of hydrous ferric oxide to goethite. Similarly, pH_{PZC} shifts to lower values have been observed for silica surfaces (Foissy and Persello, 1998). The shifts for silica were explained by an increase of surface-site acidity with polymerization and structuration (Strazhesko et al., 1974; Milonjić, 1987; Foissy and Persello, 1998). Possibly, the acidity of sulfide surface groups increases with crystallinity as well. It is proposed here that the pristine FeS surface has a pH_{PZC} ~7.5. The surface charge of FeS will also be affected by the ratio of iron to sulfide in solution. Both are potential determining ions for the pristine FeS surface (e.g. Dekkers and Schoonen, 1994; Bebié et al., 1998). In natural environments, the FeS surface charge will further depend on the solution chemistry and cation or ligand adsorption. Future work aiming to resolve the existing disagreements on the point of zero charge of metal sulfides should encompass both potentiometric titrations and electrokinetic studies, as a function of iron to sulfide ratios, and focus on ageing and exchange effects.

4.3. Surface Reactive Sites

At iron sulfide surfaces, two possible functional groups have previously been suggested: an iron(II) hydroxyl functional group, $\equiv FeOH^0$, and a sulfide functional group, $\equiv SH^0$ (Kornicker, 1988; Bebié et al., 1998). However, in solutions saturated with respect to FeS, the aqueous $FeSH^+$ complex is dominant over the $FeOH^+$ complex at pH < ~10. Thus, the Fe–SH bond is expected to be favored over Fe–OH bond. Therefore, it is proposed that the hydrated disordered mackinawite surface can be described by mono- and tri-coordinated sulfur sites as the surface reactive sites rather than the tri-coordinated iron and sulfur sites from a truncated mackinawite lattice.

Analogous to the multi-site complexation model for metal (hydr)oxides (Hiemstra et al., 1996), a model describing the proton affinity characteristics of the FeS reactive surface groups can be developed, based on crystal structural considerations. At a local level, the structure of disordered mackinawite is similar to the layered structure of crystalline mackinawite, as shown by XRPD data (Wolthers et al., 2003). In each layer FeS_4 tetrahedra are linked by edge sharing to four neighboring tetrahedra and by corner sharing to four neighboring tetrahedra (Fig. 3). The Fe–S distance is 2.230 Å and the S–Fe–S angle is that of a regular tetrahedron, i.e. 109° (Taylor and Finger, 1970). Mackinawite has a platy habit, which is determined by two (001) faces, two (100) and two (010) faces—the latter two are in fact identical—and it is assumed that disordered mackinawite consists of nano-sized crystals of the same habit (Wolthers et al., 2003). According to Wolthers et al. (2003), the dominant (~80%) crystal size in freeze-dried FeS is 7.4 × 7.4 × 2.9 nm. Assuming a perfectly platy crystal with these dimensions, this crystal will have 2 (001) faces consisting of 324 (Fe_4S) surface groups each and 2 (100) and 2 (101) faces with zero (Fe_4S), 90 (Fe_3S), 5 (Fe_2S) and 100 (FeS) surface groups each. The (Fe_4S) are coordinatively saturated and will not protonate, the (Fe_2S) are insignificant in amount compared to the (Fe_3S) and (FeS) groups. The latter two therefore determine the surface reactivity of a perfectly platy crystal and, as a close approximation, determine the surface reactivity of any FeS surface. The ratio of the concentrations of these two groups is approximately one to one. The overall reactive-site density is 4.0 sites nm^{-2}, for the reactive (100) and (010) edge faces only it is 9.1 sites nm^{-2}.

Hiemstra et al. (1996) showed that, for stable ionic solids, the charge distribution over surface groups can be described using Pauling's bond valence theory (1939, 1960), even though the actual charge will deviate from the charge predicted by this theory. The deviation will be stronger for disordered mackinawite, a solid with dominantly covalent bonds (Pauling, 1970). Nevertheless, Pauling's bond valence theory will be used here to estimate the average charge distribution at the surface of disordered mackinawite. The bond valence is +0.5 for each iron

and –0.5 for each sulfur, and thus the terminal mono-coordinated sulfur has a partial charge of –1.5, that is, –2 for the charge of a sulfide ion plus +0.5 for the S–Fe bond. Accordingly, the sulfur atom coordinated to three Fe atoms has a valence charge of –0.5. Upon hydrolysis, the terminal sulfur atoms will be protonated and the point of zero net proton charge (PZNPC) could be represented by two different configurations (Fig. 4a and 4b) or a combination of both (Fig. 4c). Macroscopically, the three configurations in Fig. 4 are equivalent.
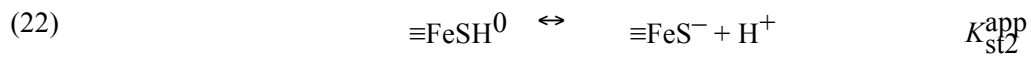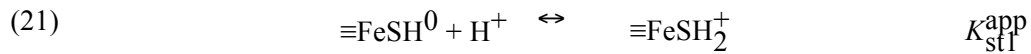
The differences in partial charge for the mono- and tri-coordinated sulfur sites will be expressed in different proton affinities. Hiemstra et al. (1996) have established a microscopic model for the surface of goethite. The goethite structure consists of double chains of edge-sharing octhedra. At the goethite surface, the mono- and tri-coordinated oxygen proton-reactive sites have very different proton affinities (Hiemstra et al., 1996) due to their different degrees of coordinative saturation. Similarly, the mono-coordinated sulfur site is expected to be the more strongly acidic surface site and determine the acid–base properties of the FeS at pH < PZNPC, while at higher pH the weaker acidic, tri-coordinated sulfur is thought to determine surface charge changes. The hydrated sulfide surface can thus be represented by a uniform array of two types of surface sites with equal concentrations: one with a relatively higher proton-affinity (the mono-coordinated sulfur site, also referred to below as the strong site) and one with a relatively lower proton affinity (the tri-coordinated sulfur site, also referred to below as the weak site). This does not mean that all strong or weak surface sites must be microscopically identical, but rather that it is possible to assign macroscopically meaningful average properties to the sites.

4.4. Surface Complexation Modeling

In keeping with the fundamental concepts for all surface complexation models (Dzombak and Morel, 1990), it is assumed that: (i) sorption reactions at the sulfide–water interface takes

22

place at specific coordination sites; (ii) sorption reactions on sulfides can be described quantitatively via mass law equations; (iii) surface charge results from the sorption reactions themselves; and (iv) the effect of surface charge on sorption can be taken into account by applying a correction factor derived from the electric double-layer theory to mass law constants for surface reactions. In the present case, the constant-capacitance model, a simplified form of the diffuse-layer model, is used to take into account the effect of surface charge on proton sorption.

A model describing the surface protonation with only one type of surface functional group was tested first, but provided a poor fit compared to the model with two site types with different proton affinities. It is therefore concluded that the experimental data show the presence of at least two site types. This is consistent with the two types of theoretically deduced reactive sites (section 4.3). The two sites were assumed to protonate and deprotonate according to the following surface protonation reactions:

(21) $$\equiv \text{FeSH}^0 + \text{H}^+ \quad \leftrightarrow \quad \equiv \text{FeSH}_2^+ \qquad K_{st1}^{app}$$

(22) $$\equiv \text{FeSH}^0 \quad \leftrightarrow \quad \equiv \text{FeS}^- + \text{H}^+ \qquad K_{st2}^{app}$$

(23) $$\equiv \text{Fe}_3\text{SH}^0 + \text{H}^+ \quad \leftrightarrow \quad \equiv \text{Fe}_3\text{SH}_2^+ \qquad K_{wk1}^{app}$$

(24) $$\equiv \text{Fe}_3\text{SH}^0 \quad \leftrightarrow \quad \equiv \text{Fe}_3\text{S}^- + \text{H}^+ \qquad K_{wk2}^{app}$$
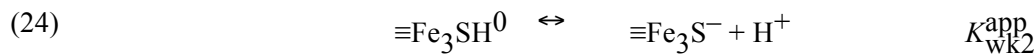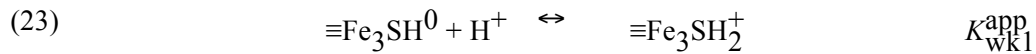
where $\equiv \text{FeSH}^0$ is the neutral, strongly acidic mono-coordinated surface functional sulfide group which can protonate (reaction 21) and deprotonate (reaction 22) and $\equiv \text{Fe}_3\text{SH}^0$ is a neutral, weakly acidic tri-coordinated sulfur sites which can protonate (reaction 23) and deprotonate (reaction 24). K_{st1}^{app}, K_{st2}^{app}, K_{wk1}^{app} and K_{wk2}^{app} are the apparent surface acidity constants and are variable model parameters. In Wolthers et al. (2003), a specific surface area of 350 $\text{m}^2 \text{ g}^{-1}$ for disordered mackinawite was proposed. Above, it was estimated that the total reactive-site density is 4.0 sites nm^{-2} and the relative site-density ratio $\equiv \text{FeSH}^0 : \equiv \text{Fe}_3\text{SH}^0$ is approximately 1:1. From these data, the concentration of both reactive

sites can be calculated: $[\equiv FeSH^0] = [\equiv Fe_3SH^0] \approx 1.2$ mmol g^{-1} FeS. This was used as input into the surface complexation model. Modeling was performed throughout at the actual FeS concentrations.

A stepwise approach to modeling the surface protonation curve (Q versus pH), derived from the titration data was adopted by considering the simple, chemically reasonable, model given by equations (21) – (24) and finding a best fit by eye to the titration curve. In each step, the computer program MINEQL+$^{©}$ 4.06 was used to calculate the surface speciation from estimated K values for Equations 21 – 24, using the constant capacitance model with a specific capacitance k of 1 Fm^{-2}. From the modeled surface speciation the surface charge was calculated as follows:

(25)
$$Q_{MINEQL} = [\equiv FeSH_2^+] + [\equiv Fe_3SH_2^+] - [\equiv FeS^-] - [\equiv Fe_3S^-]$$

and compared to experimental values. Through trial and error a set of apparent surface acidity constants for equations (21) – (24) corresponding to the best fit of the experimental surface charge was obtained. In this way, the surface protonation data derived from a titration at 0.053 M ionic strength was fitted with the MINEQL+ model. The best fit to the surface protonation curve, shown as a solid line in Fig. 5a, was obtained with the surface speciation given in Fig. 5b using the apparent surface acidity constants listed in Table 2. The apparent surface acidity constants equations (21) – (24) are interdependent (Table 2). Within a certain range, equally good fits were obtained by simultaneously increasing one apparent surface acidity constant and decreasing another. This interdependence is reflected in the error given for the constants in Table 2. The sensitivity of the model towards the specific capacitance was insignificant. An equally good fit could be obtained when increasing the k from 1 to 30 F m^{-2}. Insensitivity of the model to the specific capacitance means that the surface charge has no strong effect on the surface acidity constants. Furthermore, high ($\gg$ 1 F m^{-2}) capacitance values have, for example, been reported for ZnS ($\geq$ 100 F m^{-2}; Rönngren et al., 1991), and carbonate minerals

(30–168 F m^{-2}; Van Cappellen et al. (1993). Physically, high specific capacitance values indicate a thin and highly structured double layer, which is capable of accommodating high charge densities (e.g., Van Cappellen et al., 1993). In contrast, capacitance values for metal (hydr)oxides and silica are typically on the order of 1 F m^{-2}.

A limited number of previous studies have described the surface acid–base chemistry of other metal sulfides in terms of surface protonation reactions and surface acidity constants (see Table 3 for a summary). Rönngren et al. (1991) and Sun et al. (1991) constructed comparable models for the surface speciation of zinc and lead sulfides. In their models, the surface is described by: (i) one type of sulfide site, $\equiv$ZnS or $\equiv$PbS, which can take up one proton; (ii) one type of metal site, $\equiv$SZn or $\equiv$SPb, which can hydroxylate; and (iii) an ion exchange reaction where one cation from the solid is exchanged for two protons. They both found the amount of dissolved divalent metal cations to increase linearly with increasing solid concentration. Combined with an observed ratio of adsorbed protons per released cations close to one and a low total dissolved sulfur concentration, this result led them to conclude that the interaction of protons with the hydrous zinc and lead sulfide surfaces involves the desorption of cations. Our data do not support or refute such an ion exchange reaction. However, since the solubility of disordered mackinawite is far higher than of the lead and zinc sulfides they studied, it is expected that congruent dissolution is the dominant iron releasing mechanism.

The value for the surface acidity constant K_{st2}^{app} reported here, $10^{-6.5}$, is comparable with the value found by Rönngren et al. (1991) and Sun et al. (1991) for the same surface protonation reaction on zinc, $10^{-7.0}$, and lead, $10^{-7.1}$, sulfide surfaces (Table 3). The value for K_{wk2}^{app} of $< 10^{-9.5}$ reported here could not be constrained more precisely, due to the small impact of this value on the fit to the titration curve. In other words, changing the value of K_{wk2}^{app} to even

smaller values than $10^{-9.5}$ does not affect the goodness of fit. This indicates that the negatively charged weak surface site is not important at the surface in the pH range 6–8. Similar values for $K_{\mathrm{wk2}}^{\mathrm{app}}$ were found by Rönngren et al. (1991) and Sun et al. (1991) for the same surface protonation reaction on zinc, $10^{-10.3}$, and lead, $10^{-10.1}$, sulfide surfaces (Table 3). The reactions described by K_1^{app} for the strong and the weak sites have not been observed on zinc and lead sulfide surfaces by Rönngren et al. (1991) and Sun et al. (1991).

4.5. The Physico-Chemical Nature Of The Surface Complexation Model

The surface charge data derived from acid–base titrations can be fitted by a surface complexation model based on crystal structural considerations. The actual structure of the doubly protonated weak surface site is unclear however. In Table 2 and reaction (23), it is represented as $\equiv \mathrm{Fe_3SH_2^+}$. This would mean that the sulfide is coordinated to five atoms, while sulfide in the mackinawite structure has a coordination number (C.N.) of four. Note that higher coordination numbers of sulfide can be found in, for example, hexagonal pyrrhotite and troilite (C.N. = 6; e.g. Lennie and Vaughan, 1996). An explanation of the apparent 5-fold coordination of sulfide in $\equiv \mathrm{Fe_3SH_2^+}$ could be that the second proton is not directly bonded to the sulfur atom but located nearby in the diffuse boundary layer, hence contributing to surface charging. Alternatively, it may be envisioned that one of the Fe–S bonds in $\equiv \mathrm{Fe_3SH_2^+}$ is broken to facilitate double protonation of the sulfide. Nevertheless, the asymmetrical surface charge curves (Fig. 2a and 2b) indicate the presence of at least two types of sites. Using the site densities derived from the crystal structure of FeS, both sites should show double protonation to allow for the observed charge build-up toward lower pH values.

The surface complexation model proposed here does not take into account surface heterogeneities such as kink and step sites (e.g. Stumm, 1991), nor non-stoichiometries, and the physical-chemical nature of the actual surface remains unknown. However, the proposed model represents a first description of the surface chemistry of disordered mackinawite. The model is amenable to refinement, especially after existing disagreements on the point of zero charge of metal sulfides have been resolved through combining potentiometric titrations with electrokinetic studies, and after spectroscopic analyses have given further insight into the surface site structures and speciation.

REFERENCES

Arakaki T., Morse J.W. (1993) Coprecipitation and adsorption of Mn(II) with mackinawite (FeS) under conditions similar to those found in anoxic sediments. *Geochim. Cosmochim. Acta* **57**, 9–14.

Bayens B., Bradbury M.H. (1997) A mechanistic description of Ni and Zn sorption on Na-montmorillonite Part I: Titration and sorption measurements. *J. Contam. Hydr.* **27**, 199–222.

Bebié J., Schoonen M.A.A., Fuhrman M., Strongin D.R. (1998) Surface charge development on transition metal sulfides: An electrokinetic study. *Geochim. Cosmochim. Acta* **62**, 633–642.

Benning L., Wilkin R.T., Barnes H.L. (2000) Reaction pathways in the Fe–S system below 100°C. *Chem. Geol.* **167**, 25–51.

Berner R.A. (1967) Diagenesis of iron sulfide in recent marine sediments. *Estuaries [papers of a conference on estuaries, Jekyll Island, 1964]*, Lauff, George H. (ed), publ. Washington, American Association for the Advancement of Science, pp 268–272.

Charlet L., Wersin P., Stumm W. (1990) Surface charge of $MnCO_3$ and $FeCO_3$. *Geochim. Cosmochim. Acta* **54**, 2329–2336.

Davison W. (1991) The solubility of iron sulfides in synthetic and natural waters at ambient temperature. *Aquat. Sci.* **53**, 309–329.

Davison W., Philips N., Tabner B.J. (1999) Soluble iron sulfide species in natural waters: reappraisal of their stoichiometry and stability constants. *Aquat. Sci.* **61**, 23–43.

Dekkers M.J., Schoonen M.A.A. (1994) An electrokinetic study of synthetic greigite and pyrrhotite. *Geochim. Cosmochim. Acta* **58**, 4147–4153.

Dzombak D.A., Morel F.M.M. (1990) *Surface Complexation Modelling, Hydrous Ferric Oxide*, Wiley & Sons, NY, 393 p.

Foissy A., Persello J. (1998) Chapter 4B, Surface group ionization on silicas. In: A.P. Legrand (Ed.), *The surface properties of silicas*, Wiley & Sons, New York, pp 365–414.

Gabriel U., Gaudet J.P., Spadini L., Charlet L. (1998) Reactive transport of uranyl in a goethite column: an experimental and modelling study. *Chem. Geol.* **151**, 107–128.

Herbert Jr. R.B., Benner S.G., Pratt A.R., Blowes D.W. (1998) Surface chemistry and morphology of poorly crystalline iron sulfides precipitated in media containing sulfate-reducing bacteria. *Chem. Geol.* **144**, 87–97.

Hiemstra T., Venema P., Van Riemsdijk W.H. (1996) Intrinsic proton affinity of reactive surface groups of metal (hydr)oxides: the bond valence principle. *J. Coll. Interface Sci.* **184**, 680–692.

Kornicker W.A. (1988) Interactions of divalent cations with pyrite and mackinawite in seawater and sodium–chloride solutions. Ph.D. thesis Texas A&M University.

Kuo S., McNeal B.L. (1984) Effects of pH and Phosphate on cadmium sorption by a hydrous ferric oxide. *Soil Sci. Soc. Am. J.* **48**, 1040–1044.

Lennie A.R. and Vaughan D.J. (1996) Spectroscopic studies of iron sulfide formation and phase relations at low temperatures. *Min. Spectr., special publ.* **5**, 117–131.

Luther III G.W. (1991) Pyrite synthesis via polysulfide compounds. *Geochim. Cosmochim. Acta* **55**, 2839–2849.

Luther G.W., Ferdelman T.G. (1993) Voltammetric characterization of iron(II) sulfide complexes in laboratory solutions and in marine waters and porewaters. *Envir. Sci. Technol.* **27**, 1154–1163.

Luther III G.W., Rickard D., Theberge S., Olroyd A. (1996) Determination of Metal (Bi)Sulfide Stability Constants of Mn^{2+}, Fe^{2+}, Co^{2+}, Ni^{2+}, Cu^{2+} and Zn^{2+} by Voltammetric Methods. *Envir. Sci. Technol.* **30**, 671–679 .

Milonjić S.K. (1987) Determination of surface ionization and complexation constants at colloidal silica/electrolyte interface. *Colloids Surf.* **23**, 301–312.

Morel F.M.M., Hering J.G. (1993) *Principles and applications of aquatic chemistry*. Wiley and Sons, New York, 588 p.

Morse J.W., Arakaki T. (1993) Adsorption and coprecipitation of divalent metals with mackinawite (FeS). *Geochim. Cosmochim. Acta* **57**, 3635–3640.

Morse J.W., Luther III, G.W. (1999) Chemical influences on trace metal-sulfide interactions in anoxic sediments. *Geochim. Cosmochim. Acta* **63**, 3373–3378.

Morse J.W., Millero F.J., Cornwell J.C., Rickard D. (1987) The Chemistry of the Hydrogen Sulfide and Iron Sulfide Systems in Natural Waters. *Earth–Sci. Rev.* **24**, 1–42.

Park S.W., Huang C.P. (1987) The surface acidity of hydrous CdS. *J. Colloid and Interface Sci.* **117**, 431–441.

Pauling L. (1939, 1960) *The nature of the chemical bond*, 1st and 3rd editions, Cornell Univ. Press.

Pauling L. (1970) Crystallography and chemical bonding of sulfide minerals. *Min. Soc. Am. Spec. Pap.* **3**, 125–131.

Prasad B. (1976) Charge characteristics and phosphate adsorption on ferruginous soils and synthetic iron oxides. Ph.D. Thesis, Univ. Minnesota.

Renders P.J., Seward T.M. (1989) The adsorption of thio gold(I) complexes by amorphous As_2S_3 and Sb_2S_3 at 25 and 90°C. *Geochim. Cosmochim. Acta* **53**, 255–267.

Rickard D. (1989) Experimental concentration–time curves for the iron(II) sulfide precipitation process in aqueous solutions and their interpretation. *Chem. Geol.* **78**, 315–324.

Rickard D. (1995) Kinetics of FeS precipitation: Part 1. Competing reaction mechanisms. *Geochim. Cosmochim. Acta* **59**, 4367–4379.

Rickard D., Luther III G.W. (1997) Kinetics of pyrite formation by the H_2S oxidation of iron (II) monosulfide in aqueous solutions between 25 and 125ºC: The mechanism. *Geochim. Cosmochim. Acta* **61**, 135–147.

Rönngren L., Sjöberg S., Sun Z., Forsling W., Schindler P.W. (1991) Ion exchange and acid/base reactions at the ZnS–H_2O interface. *J. Colloid and Interface Sci.* **145**, 396–404.

Schulthess C.P., Sparks D.L. (1986) Backtitration technique for proton isotherm modeling of oxide surfaces. *Soil Sci. Soc. Am. J.* **50**, 1406–1411.

Spadini L., Bott M., Wehrli B., Manceau A. (2003). Analysis of the major Fe bearing phases in recent lake sediments by EXAFS spectroscopy. *Aquat. Geochem.* **9**, 1–17.

Sposito G. (1984) *The surface chemistry of soils*. Oxford U.P., New York, p 234.

Strazhesko D.N., Strelko V.B., Belyakov V.N., Rubanik S.C. (1974) Mechanism of cation exchange on silica gels. *J. Chromatogr.* **102**, 191–195.

Stumm W. (1991) *Chemistry of the solid–water interface, processes at the mineral–water and particle–water interface in natural systems*. Wiley & Sons, NY, 428 p.

Stumm W., Morgan J.J. (1981) *Aquatic Chemistry*. Wiley-Interscience, New York. p 681.

Suleimonov O.M., Seward T.M. (1997) A spectrophotometric study of hydrogen sulfide ionisation in aqueous solutions to 350°C. *Geochim. Cosmochim. Acta* **61**, 5187–5198.

Sun Z.X., Forsling W., Rönngren L., Sjöberg S., Schindler P.W. (1991) Surface reactions in aqueous metal sulfide systems. 3. Ion exchange and acid/base properties of hydrous lead sulfide. *Colloids and Surf.* **59**, 243–254.

Taylor L.A., Finger L.W. (1970) Structural refinement and composition of mackinawite. *Carnegie Inst. Washington Geophys. Lab. Ann. Rep.* **69**, 318–322.

Van Cappellen P., Charlet L., Stumm W., Wersin P. (1993) A surface complexation model of the carbonate mineral–aqueous solution interface. *Geochim. Cosmochim. Acta* **57**, 3505–3518.

Viollier E., Inglett P.W., Hunter K., Roychoudhury A.N., Van Cappellen P. (2000) The ferrozine method revisited: Fe(II)–Fe(III) determination in natural waters. *Appl. Geochem.* **15**, 785–790.

Watson J.H.P., Cressey B.A., Roberts A.P., Ellwood D.C., Charnock J.M., Soper A.K. (2000) Structural and magnetic studies on heavy-metal-adsorbing iron sulphide nanoparticles produced by sulphate-reducing bacteria. *J. of Magn. and Magn. Materials* **214**, 13–30.

Wharton M.J., Atkins B., Charnock J.M., Livens F.R., Pattrick R.A.D., Collison D. (2000) An X-ray absorption spectroscopy study of the coprecipitation of Tc and Re with mackinawite (FeS). *Appl. Geochem.* **15**, 347–354.

Widler A.M., Seward T.M. (2002) The adsorption of gold(I) hydrosulphide complexes by iron sulfide surfaces. *Geochim. Cosmochim. Acta* **66**, 383–402.

Wolthers M., van der Gaast S.J., Rickard D. (2003) The structure of disordered mackinawite. *Am. Mineral.* **88**, 2007–2015.

Zhang J.–Z, Millero F.J. (1994) Investigation of metal sulfide complexes in sea water using cathodic stripping square wave voltammetry. *Analyt. Chim. Acta* **284**, 497–504.

TABLES

Table 1. Properties of disordered mackinawite (Wolthers et al., 2003). SSA = specific surface area; average diameter = the average primary particle size, site density = the density of sites at the surface; [$\equiv$FeS] = the concentration of mono-coordinated sulfur sites at the surface; [$\equiv$Fe$_3$S] = the concentration of tri-coordinated sulfur sites at the surface.

SSA $(m^2\,g^{-1})$	Average diameter (nm)	Site density (sites nm^{-2})	[$\equiv$FeS] (mmol g^{-1}FeS)	[$\equiv$Fe$_3$S] (mmol g^{-1}FeS)
350	4.2 ± 0.2	4.0	1.2	1.2

Table 2. Model surface protonation reactions and their estimated apparent equilibrium constants derived from the model fit shown in Fig. 5a. The surface speciation based on these data is shown in Fig. 5b.

Model reactions	LogK
$\equiv FeSH^0 + H^+ \leftrightarrow \equiv FeSH_2^+$	$LogK_{st1}^{app} = +8.0 \pm 0.1$
$\equiv FeSH^0 \leftrightarrow \equiv FeS^- + H^+$	$LogK_{st2}^{app} = -6.5 \pm 0.1$
$\equiv Fe_3SH^0 + H^+ \leftrightarrow \equiv Fe_3SH_2^+$	$LogK_{wk1}^{app} = +7.85 \pm 0.05$
$\equiv Fe_3SH^0 \leftrightarrow \equiv Fe_3S^- + H^+$	$LogK_{wk2}^{app} < -9.5$

Table 3. Recommended surface protonation reactions and estimated apparent equilibrium constants from: [1] this study; [2] Rönngren et al., 1991; [3] Sun et al., 1991.

Reaction	LogK	Reference
$(\equiv FeS)H^0 + H^+ \leftrightarrow (\equiv FeS)H_2^+$	$+8.0 \pm 0.1$	[1]
$(\equiv FeS)H^0 \leftrightarrow (\equiv FeS)^- + H^+$	-6.5 ± 0.1	[1]
$(\equiv Fe_3S)H^0 + H^+ \leftrightarrow (\equiv Fe_3S)H_2^+$	$+7.85 \pm 0.05$	[1]
$(\equiv Fe_3S)H^0 \leftrightarrow (\equiv Fe_3S)^- + H^+$	< -9.5	[1]
$\equiv SZn^0 + 2H^+ \leftrightarrow \equiv SH_2^0 + Zn^{2+}$	9.59 ± 0.03	for synthetic ZnS, [2]
	9.65 ± 0.03	for sphalerite, [2]
$\equiv SZn^0 + H_2O \leftrightarrow \equiv SZnOH^- + H^+$	-10.28 ± 0.10	for synthetic ZnS, [2]
	-10.29 ± 0.10	for sphalerite, [2]
$\equiv ZnS^0 + H^+ \leftrightarrow \equiv ZnSH^+$	6.91 ± 0.03	for synthetic ZnS, [2]
	7.14 ± 0.03	for sphalerite, [2]
$\equiv SPb^0 + 2H^+ \leftrightarrow \equiv SH_2^0 + Pb^{2+}$	9.48 ± 0.027	for synthetic PbS, [3]
	10.21 ± 0.024	for galena, [3]
$\equiv SPb^0 + H_2O \leftrightarrow \equiv SPbOH^- + H^+$	-10.0 ± 0.09	for synthetic PbS, [3]
	-10.2 ± 0.09	for galena, [3]
$\equiv PbS^0 + H^+ \leftrightarrow \equiv PbSH^+$	7.11 ± 0.044	for synthetic PbS, [3]
	7.15 ± 0.047	for galena, [3]

FIGURE CAPTIONS

Figure 1. Total dissolved Fe(II), log[Fe(aq)$_T$], plotted versus pH. Filled diamonds are measured values; the dotted line is the predicted total dissolved iron using the solubility $K_S^* = 10^{+3.98}$ (Davison et al., 1999) and the solid lines using $K_S^{app} = 10^{+4.87\pm0.27}$ (this work), fitting the log[Fe(aq)$_T$] data with $R^2 = 0.90$ (see sections 2.2 and 3.1).

Figure 2. Proton balances from the disordered mackinawite surface titrations: (a) experimental proton balance Q calculated according to equation (2) from the titrations performed at $I = 0.053$ M plotted versus pH; (b) Q calculated from $I = 0.0078$ M (open triangles) and $I = 0.103$ M (filled squares, duplicate experiment plotted as one) titrations versus pH.

Figure 3. Sketch of the mackinawite structure viewed from ca 30° above the (001) plane. The tetragonal unit cell is indicated. The Fe–Fe bond length is 2.60Å which is extremely close to that of α-iron and suggests significant Fe–Fe bonding. The Fe atoms are in square planar coordination and constitute the (001) plane of the structure. The sheets of Fe atoms are separated by ca. 0.5 nm and the sheets are weakly held by Van der Waals bonding between the S atoms. The interstices between the sheets are potential sites for other molecules such as H_2O. The sketch shows open tetrahedra with Fe atoms in the centers and S atoms at the corners. Conventional ionic radii are used for clarity. The Fe–Fe bonding, the Fe–S covalent and S–S Van der Waals bonding make substantial changes to the effective atomic radii.

Figure 4. Theoretical surface structural models at the point of zero net proton charge (PZNPC), viewed perpendicularly to the (001) plane, which is represented as tetrahedra (cf. Fig. 3). The representation of the sulfide surface is largely notional because relevant detailed surface spectroscopic data to support the presence of these various groups is lacking. The PZNPC might be represented by three configurations: (a) a double protonation of the mono-

coordinated sulfur sites and no protonation of the tri-coordinated sulfur sites; (b) single protonation of both site types; (c) or a combination of (a) and (b). Macroscopically, the three configurations in Fig. 4 are equivalent

Figure 5. Surface complexation model fit to an experimental proton balance at $I = 0.053$ M. (a) experimental Q (open circles) from an $I = 0.053$ M titration fitted with Q_{MINEQL} (solid line) from equation (9); (b) surface speciation calculated in MINEQL+ which sums up to Q_{MINEQL} fitting the experimental data in Figure 5a.
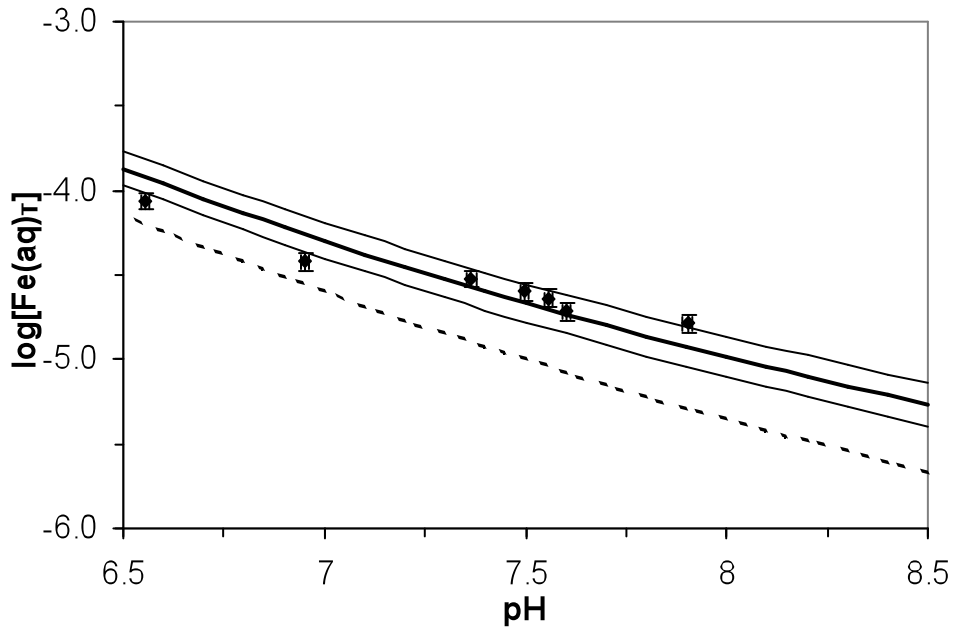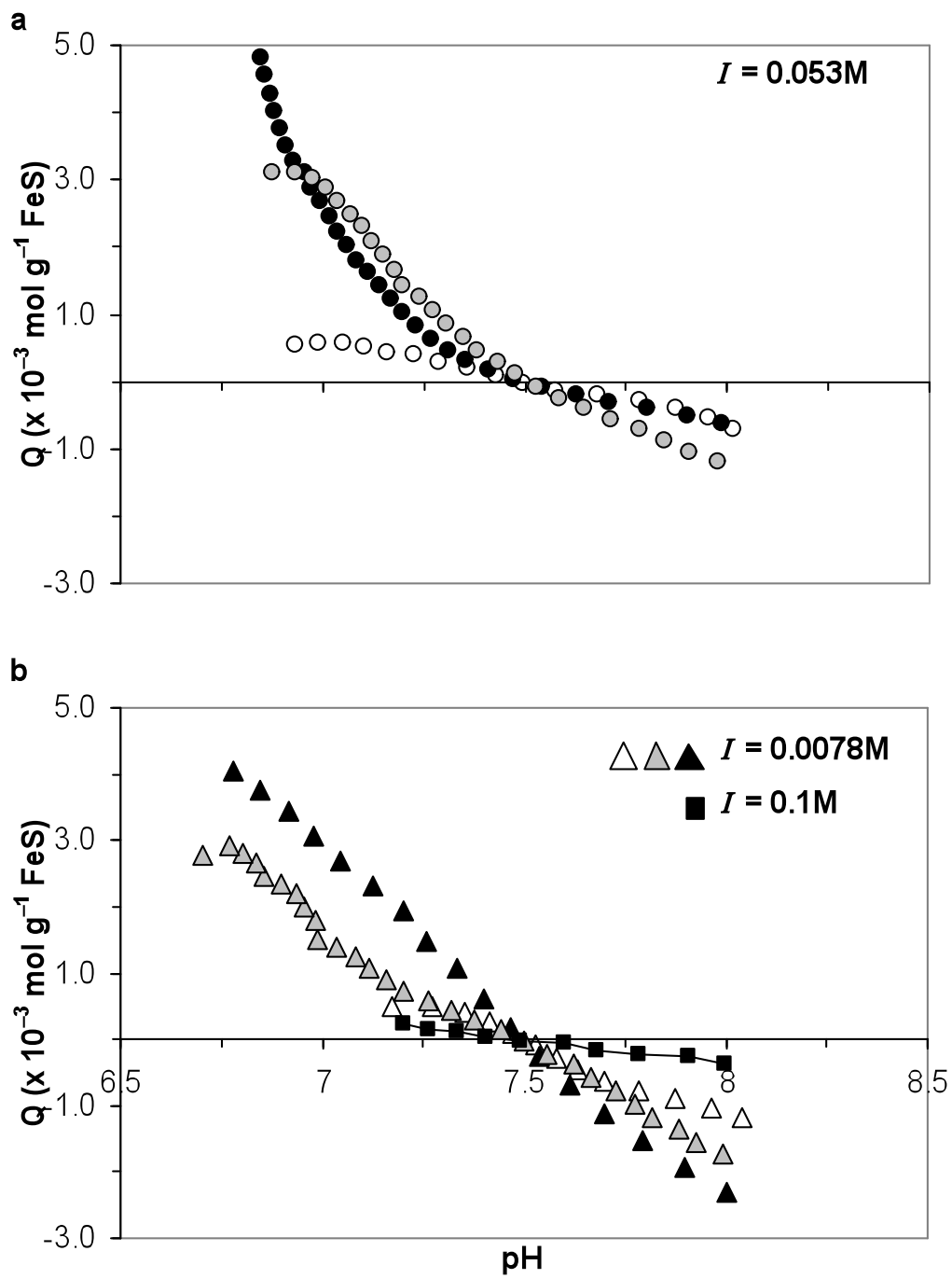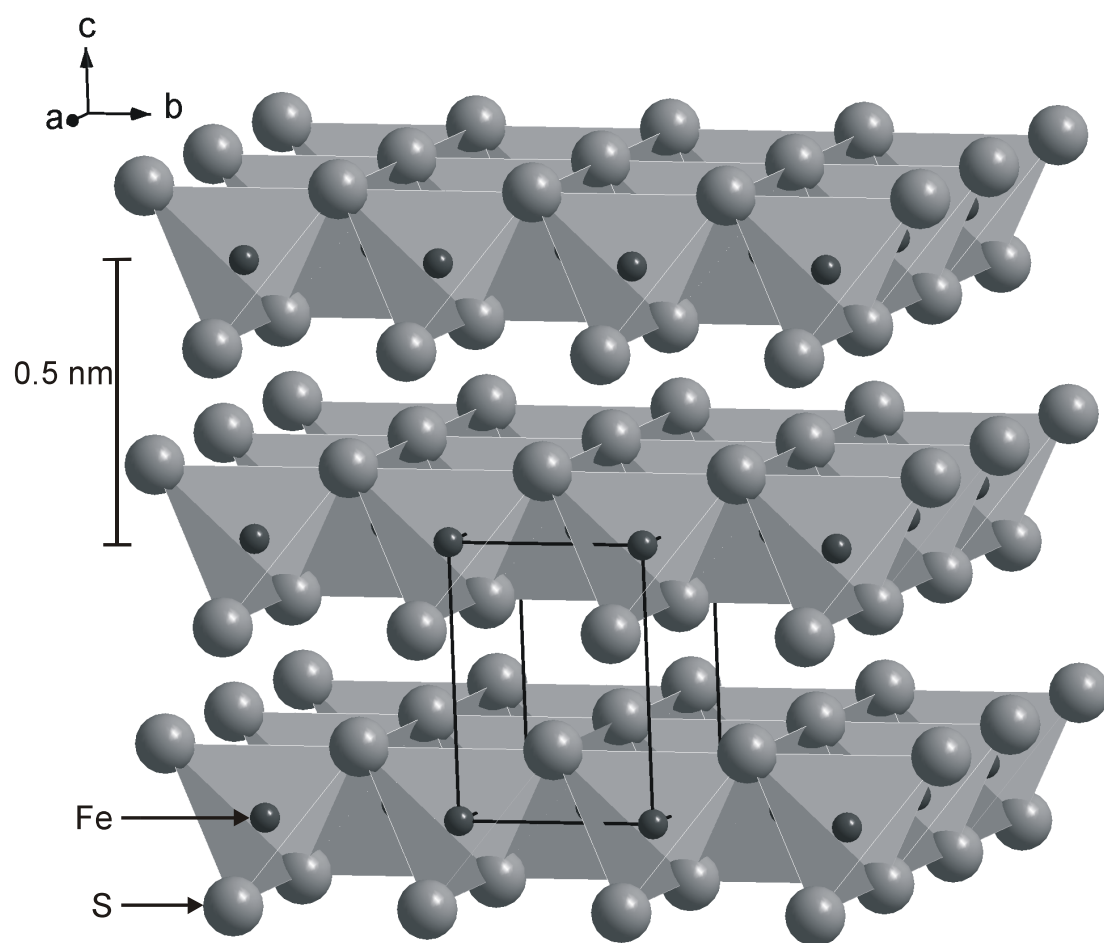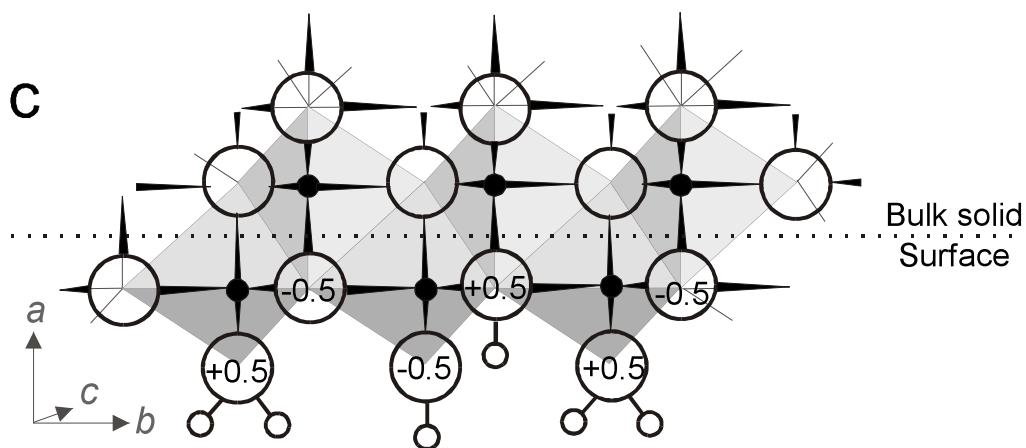
Figure 1

Figure 2

Figure 3

39

a

Bulk solid
Surface

-0.5   -0.5   -0.5

+0.5   +0.5   +0.5

a

c
b

b

Bulk solid
Surface

+0.5   +0.5   +0.5

-0.5   -0.5   -0.5

a

c
b

c

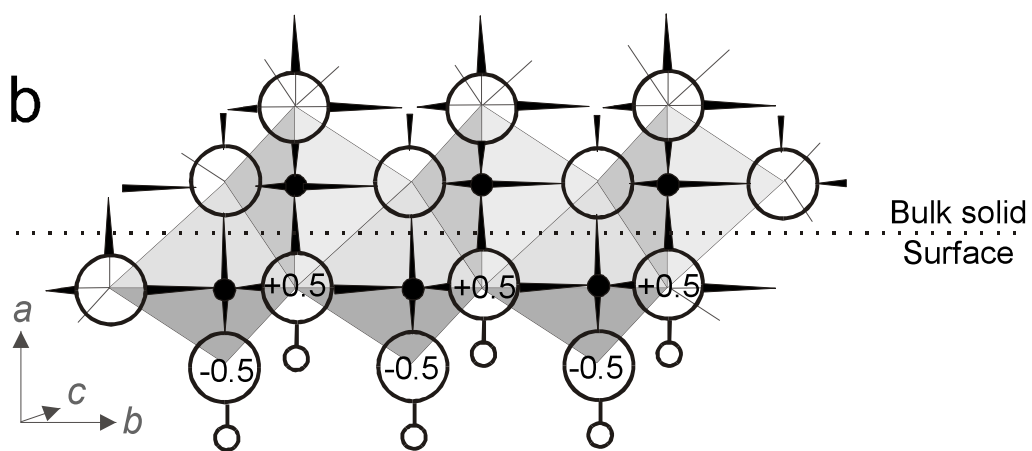Bulk solid
Surface

-0.5   +0.5   -0.5

+0.5   -0.5   +0.5

a

c
b

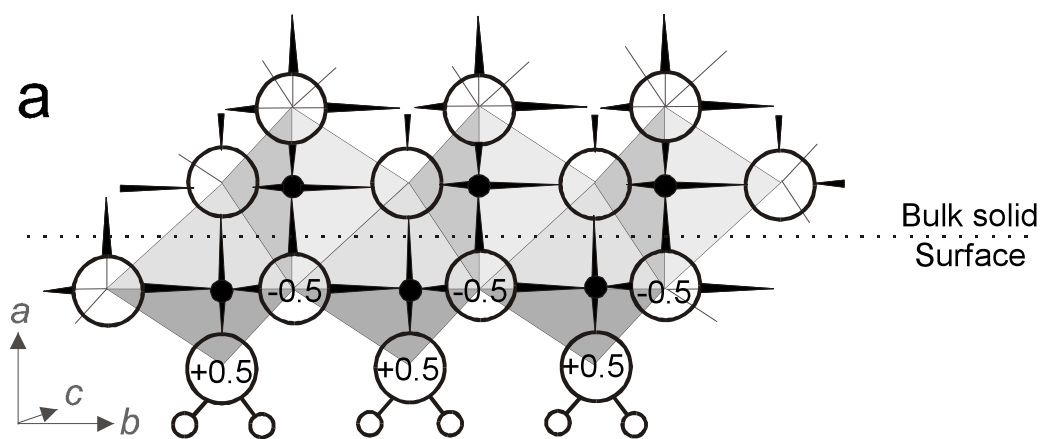(+0.5) = S atom with a partial charge of +0.5

● = Fe atom   ○ = surface proton

Figure 4

40

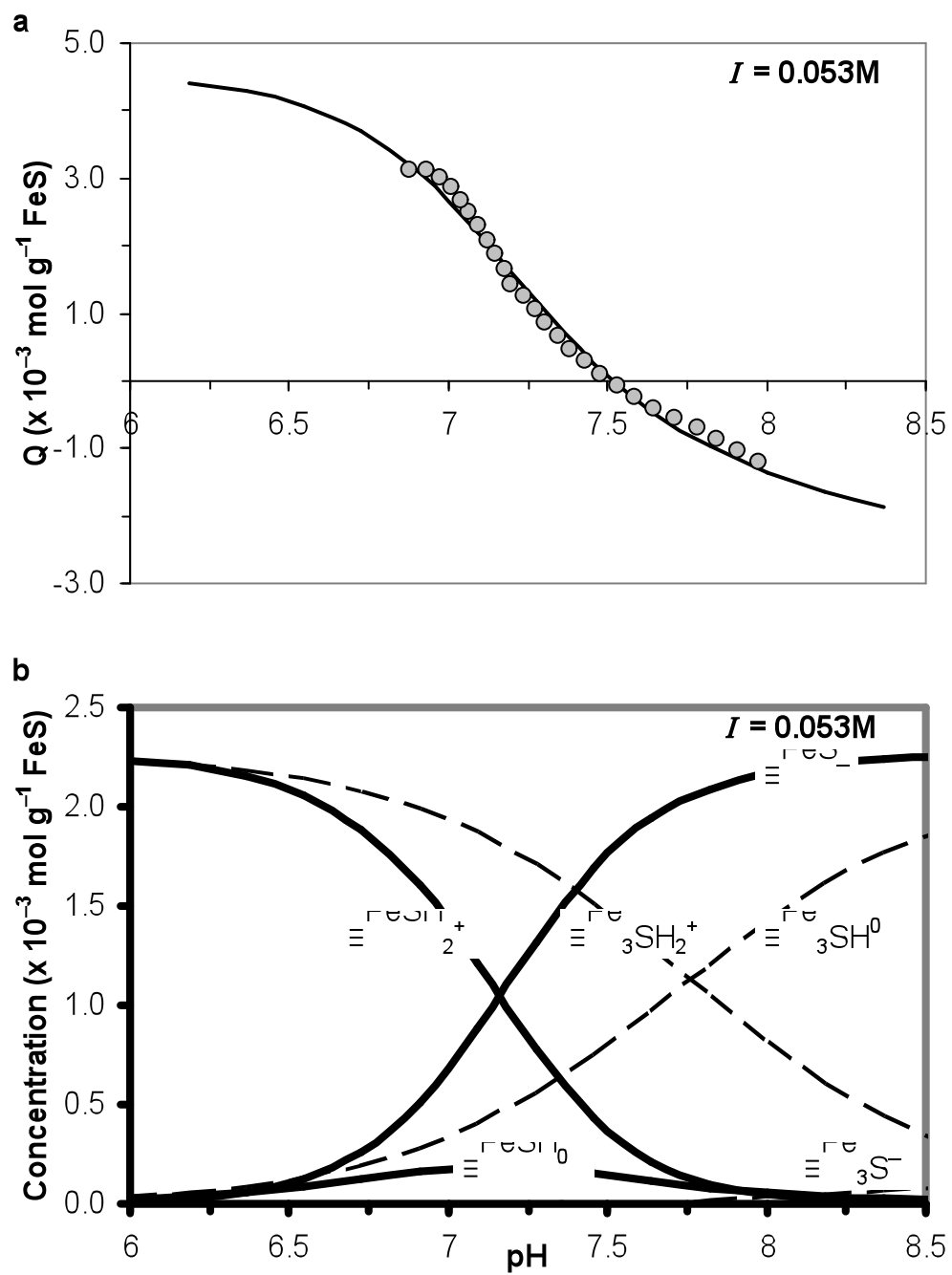**a**

$I = 0.053M$

b

$I = 0.053M$

$\equiv FeSH_2^+$

$\equiv Fe_3SH_2^+$

$\equiv Fe_3SH^0$

$\equiv FeSH^0$

$\equiv Fe_3S^-$

$\equiv FeS^-$

Figure 5